



Biogenic iron oxide nanoparticles and activated sodium persulphate for hydrocarbon remediation in contaminated soil

Oladotun P. Bolade^{a,b}, Anuoluwa A. Akinsiku^a, Oluwatobi S. Oluwafemi^c, Akan B. Williams^a, Nsikak U. Benson^{a,*}

^a Department of Chemistry, Covenant University, Ota, Nigeria

^b Department of Petroleum Chemistry, American University of Nigeria, Yola, Nigeria

^c Department of Chemical Sciences, University of Johannesburg, Johannesburg, South Africa

ARTICLE INFO

Article history:

Received 18 February 2021

Received in revised form 15 June 2021

Accepted 19 June 2021

Available online 24 June 2021

Keywords:

Central composite design

Crude oil contamination

Green synthesis

FeO nanoparticles

Sodium persulphate

Total petroleum hydrocarbon

ABSTRACT

Biogenic iron oxide nanoparticles synthesized from a locally sourced, readily available plant – *Azadirachta indica*, were used synergistically with sodium persulphate (PS) to degrade total petroleum hydrocarbons (TPHs) in contaminated soil. A chemometric approach to optimizing the conditions for the degradation of TPH was developed using central composite design (CCD). Characterization of iron oxide nanoparticles was carried out with X-ray diffraction (XRD), scanning electron microscopy (SEM), energy dispersive X-ray (EDX) spectroscopy, Fourier transform infrared spectroscopy (FTIR), transmission electron microscopy (TEM), high-resolution transmission electron microscopy (HRTEM), and selected electron area diffraction (SAED). Analysis of TPH was carried out with gas chromatography flame ionization detector (GC-FID). The optimum condition for the complete degradation of TPH was achieved at pH 6.0 and oxidant dosage of 0.74 M within 14 h and 5 days. Iron nanoparticles AZA FeNP (1:1) and AZA FeNP (2:1) were synthesized by varying the ratio of extract/precursor. The nanoparticles displayed heterogeneous, amorphous morphology with increased agglomeration in AZA FeNP (1:1). AZA FeNP (2:1) XRD spectra exhibited characteristic peaks at 27.0°, 35.4° and 44.5°, which are attributed to iron nanoparticles. TEM and HR-TEM images confirmed spherical nanoclusters' presence with an average size of 9.3 and 10.0 nm for AZA FeNP (1:1) and AZA FeNP (2:1), respectively. The EDX spectra displayed intense peaks of oxygen, carbon, and iron at 0.4, 0.6 and 6.4 KeV confirming the presence of FeNP. Under optimized conditions, PS alone degraded 68% TPH while 0.07 and 0.15 g/L FeNP achieved ~93 and 95% degradation, respectively. Additionally, 0.07 and 0.15 g/L FeNP-activated PS achieved ~99 and 100% TPH degradation, respectively. The outcome of these findings suggests that FeNP synthesized using *A. indica* successfully catalyzed PS for complete degradation of TPH in crude oil-contaminated soil.

© 2021 Elsevier B.V. All rights reserved.

1. Introduction

Petroleum hydrocarbon contamination of soil and groundwater has been widely reported, particularly in oil-rich countries like Nigeria. In most affected communities, hydrocarbon contamination has reduced the availability of arable land and potable water. Total petroleum hydrocarbons (TPHs) are frequently released into the environment as a result

* Corresponding author.

E-mail address: nbenson@covenantuniversity.edu.ng (N.U. Benson).

of oil spills, industrial accidents, and pipeline vandalism, making them significant environmental polluting organics. As a result, both local and international organizations have called for the remediation of contaminated land and aquifers. Although remediation by enhanced natural attenuation (RENA) has been widely adopted, studies have shown the ineffectiveness of this method (Sam et al., 2017; Zabbey et al., 2017). RENA has not been sufficiently effective for the destruction of a wide range of dissolved, sorbed and non-aqueous phase liquids (DNAPL). However, metal-based nanoparticles, particularly those synthesized using plant materials, have recently gained growing attention for the remediation of aromatic hydrocarbons contamination due to their unique nanoscale sizes.

In recent years, plant-based synthetic approaches for metal nanoparticles have sparked a lot of interest recently due to their environmental friendliness, rapidity of methods, and cost effectiveness, non-generation of harmful by-products, among other considerations (Bolade et al., 2021; Li et al., 2021; Rafael et al., 2021; Perveen et al., 2020; Naraginti and Li, 2017). In comparison to microbial approaches, the biosynthesis of nanoparticles utilizing plant materials has attracted a huge interest due to the stabilizing and capping effects of bioactive components of these plant extracts (Jagathesan and Rajiv, 2018). In most synthetic methods, dried and pulverized plant materials are easily extracted using different methods such as cold maceration, sonication, microwave or Soxhlet method. Hence, aqueous or organic extracts could be mixed with precursor solution depending on the type of metal nanoparticle being synthesized. Green, non-toxic synthesis methods utilizing various parts of living plants such as leaves, stems, roots and bark have been reported for the synthesis of magnetic nanoparticles. This method is environment-friendly and does not require complex reaction mechanisms (Majidi et al., 2016). Several plants including aquatic and terrestrial weeds have also been studied (Prabhakar and Samadder, 2017). Generally, green synthetic routes for production of nanomaterials facilitates toxic substances and hazardous waste minimization, reduced energy use, and promotes environmental sustainability (Kurowska-Susdorf et al., 2019; Anastas and Warner, 1998).

Although the biosynthesis of iron oxide nanoparticles using *Mikania mikrantha* (Biswas et al., 2021), *Zingiber officinale* (Kirdat et al., 2021), *Cymbopogon citratus* (Patiño Ruiz et al., 2020), *Coriandrum sativum* L. (*cilantro*) (Singh et al., 2020), *Moringa oleifera* (Tovar et al., 2020), *Carica papaya* (Bhuiyan et al., 2020); *Phoenix dactylifera* L. (Abdullah et al., 2020) leaves extracts have been reported, the green synthesis and environmental application of FeO nanoparticles synthesized using *Azadirachta indica* leaf extracts and activated sodium persulphate for remediation of petroleum contamination has not been fully explored. The biosynthesis of iron-based nanoparticles using indigenous herbs and medicinal plants high in polyphenol content has been documented (Contreras-calderón et al., 2011; Patay et al., 2016). The ability to synthesize nanoparticles in aqueous media and under standard conditions (temperature and pressure), reduces the danger of production of toxic by-products and disposal of organic waste/reagents. In particular, iron-based nanomaterials have found increasing acceptance among researchers due to their unique morphological and physicochemical properties. They are largely non-toxic and possess magnetic susceptibility. The use of biological routes for synthesis of nanoparticles presents an eco-friendly, facile and green method with wider acceptance (Prabhakar and Samadder, 2017).

Persulphates are peroxygens, which are highly reactive chemical oxidants. When these oxidants are activated, they can effectively degrade petroleum hydrocarbons in soil and water. They are activated by heat (Bolade et al., 2019a; Zheng et al., 2016), ultraviolet (UV), ultrasound, and electron beam to generate sulfate radicals (Acero et al., 2018; Matzek and Carter, 2016; Sathya et al., 2017). Other activation methods include the use of metals, alkaline solution, nanoparticles, organic/inorganic chelates and minerals (Da Silva et al., 2015). Combining different technologies such as chemical oxidation and nanoremediation in an integral or sequential strategy can help to overcome the limitation of single remediation methods. This presents a viable option for dealing with complex and high contaminant concentrations where neither nanoremediation nor chemical oxidation alone would be effective or/and cost efficient. Also, aqueous-based biosynthesis of iron nanoparticles precludes the use of toxic reagents and produces biostabilised, less aggregated nanoparticles. Additionally, they facilitate activation of persulphates resulting in catalyzed degradation of hydrocarbons (Jiemvarangkul et al., 2011; Okuo et al., 2018; Sun et al., 2018). Recent studies have shown that the effectiveness of combined techniques depend on the selection of the oxidants, oxidant dosing and the effect of oxidant on microbes and aquifer geochemistry (Lemaire et al., 2013a,b); (Wei et al., 2016). The application of peroxygens for degradation of petroleum hydrocarbon is emerging and presents a promising remediation approach among chemical oxidants. However, studies on persulphate for hydrocarbon remediation are only reported in few literatures.

Therefore, the aim of this study was to develop an effective synergistic method for the degradation of TPH in crude oil contaminated soil using biosynthesized iron oxide nanoparticles and sodium persulphate. The study objectives were (a) determination of the optimum conditions for the uncatalyzed degradation of TPH with sodium persulphate using a multivariate experimental approach based on central composite design; (b) optimization studies premised on three selected variables, including time, oxidant concentration and pH. These optimized conditions were validated by evaluating TPH concentrations in contaminated soil samples using the model equation developed under optimized settings. The iron oxide nanoparticles were then synthesized using *Azadirachta indica* leaves and morphologically characterized; (c) under optimized conditions, biosynthesized iron oxide nanoparticles were applied singly and synergistically with sodium persulphate for TPH degradation. To the best of our knowledge, this is a novel report exploring the synthesis of FeO nanoparticles using *Azadirachta indica* and activated sodium persulphate for nanoenvironmental considerations in the remediation of petroleum-contaminated soil.

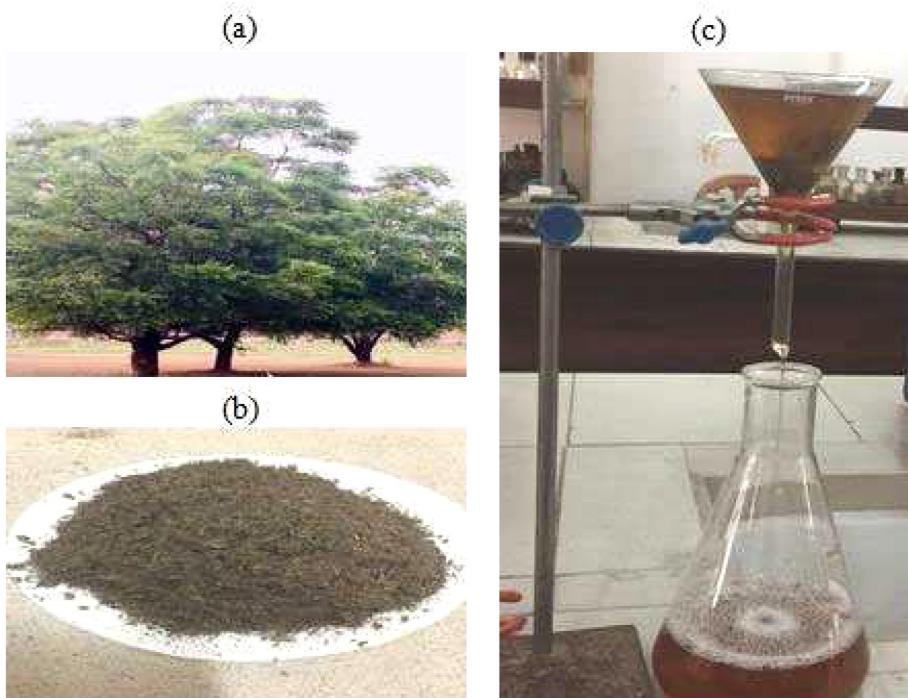


Fig. 1. *Azadirachta indica* (a) Tree plant (commonly called *Dogonyaro*) within the premises of Covenant University (b) Powdered leaves (c) Aqueous extract during filtration.

2. Materials and methods

2.1. Chemicals and reagents

Ethanol (bulk), acetone, dichloromethane (Analar grade), *n*-hexane (99%), anhydrous sodium sulfate, 5% ferric chloride, concentrated sulfuric acid, concentrated hydrochloric acid, sodium hydroxide. Hydrocarbon window defining standard was purchased from AccuStandards, USA. Complimentary crude oil was obtained from an indigenous oil company in Nigeria.

2.2. Collection and identification of plant leaves

Azadirachta indica leaves were obtained from the premises of Covenant University, Nigeria and authenticated by botanists from the Department of Biological Sciences within the University. The leaves were thoroughly washed in distilled water to remove dust particles before being air-dried at laboratory room temperature ($\sim 27^\circ\text{C}$) and in the absence of sunlight for 14 days. Dried leaves were then pulverized to powder form using a domestic blender and preserved in airtight containers until further use (Tegelberg, 2018). Pictorial representation of collection of plant leaves and preparation of extracts is presented in Fig. 1.

2.2.1. Preparation of plant extracts using different solvents

The dried powdered leaves (10 g) were exhaustively cold-extracted with distilled water (50 mL) for 72 h. The extracts were filtered with Whatman No. 41 filter paper to obtain extracts free of particles. The residue of each plant extract was re-extracted twice, filtered and the filtrates combined. The pooled filtrate of each plant extract was concentrated with the aid of vacuum rotary evaporator (BUCHI Labortech AG, Model 1, R-215) under reduced pressure and at 50°C . For GC-MS analysis, a portion of the aqueous extract was re-extracted with ethanol. The crude extracts were concentrated to 1 mL and transferred into amber colored GC vials.

2.3. Fourier transform infrared and Gas chromatography-mass spectrometry analyzes

The FTIR analysis of an aqueous extract of *A. indica* was carried out using Agilent Cary 630 FTIR (Range – $4000\text{--}650\text{ cm}^{-1}$, Resolution – 8 cm^{-1} , Microlab PC software with ATR sampling unit). The GC-MS analysis of ethanolic fraction was performed using Agilent 7890B GC coupled with Agilent 5977 Mass Spectrometer. The equipment has a HP-5MS ultra inert capillary non-polar column with dimensions of $30\text{ mm} \times 0.25\text{ mm ID} \times 0.25\text{ }\mu\text{m}$ film. The carrier gas and ionization

system used were helium with a flow of 1.0 mL/min and electron ionization of 70 eV, respectively. The injector and mass transfer lines were operated at 250 °C and 280 °C, while the oven temperature was programmed as follows: 50 °C for 1 min, then gradually increased to 300 °C at 7 °C/min for 14 mins. For each sample, 1 µL was injected with a 1:10 split ratio.

2.4. Determination of soil pH

Soil pH was determined in 1:2.5 soil–water suspension. 10 g of air-dried soil was weighed in a 50 mL beaker and mixed with deionized water (25 mL). The mixture was stirred for 20 mins and allowed to stand for 45 mins. The electrode of the pH meter was inserted into the suspension, and pH reading was taken. The pH meter was calibrated with buffers 4.0 and 7.0 before use.

2.5. Procedure for particle size determination (hydrometer method)

Particle size analysis was carried out to determine the percentage of sand, silt and clay using the hydrometer method described by [Ashworth et al. \(2001\)](#). 100 mL 5% sodium hexametaphosphate dispersing solution was added to 880 mL of deionized water. The dispersing solution was prepared by dissolving 50 g of sodium hexametaphosphate in deionized water and made up to 1 L mark. 50 g of soil was weighed and transferred into a 1 L cylinder, then filled up to mark with deionized water. Temperature and hydrometer readings were taken for blank and soil at different time intervals to determine the amount of silt and clay at 1 min and 7 h repeatedly. The description of soil texture was based on the United States Department of Agriculture (USDA) textural triangle classification system. Moreover, the following equations were used for the calculations of the respective percentages of clay, silt and sand contents (Eqn. S1).

2.6. Procedure for determination of metals in soil using MP-AES

Sample preparation procedure used for acid digestion of soil sample using the United States Environmental Protection Agency (USEPA) Method 3050B. 1 g of oven-dried (at 105 °C) soil sample was digested with 5 mL HNO₃, 15 mL H₂SO₄ and 3 mL HClO₄ by heating in a fume hood. On digestion, a dense white fume appeared. The mixture was allowed to cool, diluted with deionized water and filtered through acid-washed Whatman filter paper (No. 44). The filtrate was transferred into 50 mL beaker and made to the mark using deionized water. Metal analysis was carried out in triplicates by aspirating sample into microwave plasma-atomic emission spectrometer (Agilent 4200 MP-AES) ([USEPA, 1996](#)).

2.7. Determination of moisture content and total organic carbon (TOC)

Moisture content and TOC were determined using the method described by American Society for Testing and Materials (ASTM) Method D 2974–00. A porcelain crucible was heated in a muffle furnace for 1 h at 375 °C, cooled for 30 mins in a desiccator and weighed. Each soil sample was sieved using a 2 mm sieve and 30.00 g of sieved soil was weighed and placed in the cooled crucible. W_1 (g) and W_2 (g) were recorded as the weight of soil + crucible, respectively. The crucible and its contents were placed in the oven and dried to constant weight (at 105 °C overnight). The crucible and its contents were removed from the oven afterwards and placed in a desiccator to cool, before being weighed. Weight of soil + crucible, post-heating, was recorded as W_3 (g). Moisture content (%) was calculated using the equation (Eqn. S4).

For the determination of total organic carbon (TOC) using loss on ignition method, the soil sample and crucible (after drying in the oven for moisture content determination) were transferred into the muffle furnace, heated to 375 °C slowly and left for 16 h. The sample was allowed to cool to 150 °C, removed from the furnace and placed in a desiccator. After 30 min, the soil sample was removed from the desiccator and weighed ([American Society for Testing and Materials \(ASTM\) D2974-00, 2000](#)). This weight was recorded as W_4 (g). TOC (%) was calculated using the equation (Eqn. S5):

2.8. Design of optimization experiments

Uncontaminated soil was obtained from an excavation site within Covenant University, Nigeria, and in the laboratory, the samples were passed through a 2 mm sieve and thereafter contaminated with 40 g/kg crude oil. Each contaminated sample was then thoroughly mixed and left for 100 days. The contaminated soil was left in a dark amber bottle for this period to prevent photodegradation which facilitates aging as organic contaminants strongly adsorb to the soil. Bench-scale petroleum hydrocarbon degradation study was carried out using varying concentrations of sodium persulphate within 30 days. To achieve this, an experimental plan was developed using central composite design (Table S1). Based on the experimental design, varying concentrations of sodium persulphate were added to 10 g of contaminated soil and left for degradation to occur. The duration of degradation was varied between 1–30 days and pH adjustment was carried out using sodium hydroxide or hydrochloric acid. Upon degradation, TPH extraction was carried out on the soil. The values obtained were analyzed using response surface methodology to obtain the optimum conditions (time, pH and persulphate dosage) for degradation of TPH using sodium persulphate as an oxidant.

2.9. Extraction of total petroleum hydrocarbons from contaminated soil

Extraction of TPH was carried out using the United States Environmental Protection Agency (USEPA) Method 8015D. 10 g of contaminated soil was weighed into a pre-cleaned extraction bottle and dried with anhydrous sodium sulfate until free-flowing. 30 mL of acetone/hexane (1:1) was added. The mixture was then sonicated for 1 h at 70 °C and left to cool before filtering using glass wool. The filtrate was concentrated to 1mL using a rotary evaporator.

2.10. Procedure for synthesis of nanoparticles

Freshly prepared ferric chloride solution (0.1 N) was mixed dropwise with the plant extracts in a ratio of 1:1 and 1:2 at a flow rate of 4–8 mL/min. The solution was stirred continuously for 10 mins, and then the vials were capped to avoid oxidation. Nanoparticles formed were collected by centrifuging at 10,000 rpm for 30 mins. Nanoparticles were washed twice with deionized water and once with anhydrous ethanol. Synthesized nanoparticles were labeled as AZA FeNP 1:1 and AZA FeNP 2:1. Calcination was carried out at 600 °C.

2.10.1. Characterization of biosynthesized nanoparticles

The UV/Visible spectra of biogenic nanoparticles were recorded within the spectral range of 200–800 nm using UV-3000 ORI, Germany, to confirm the nanoparticles' formation. X-ray diffraction (XRD) analysis was carried out by coating the biosynthesized nanoparticles onto a glass slide and analyzed through Empyrean by PanAnalytical, with sample scanning within the 2θ range of 0–70°. The Debye–Scherrer equation was employed to calculate the average particle size of the synthesized nanoparticles. This gives a relationship between peak broadening in XRD and is estimated by the equation:

$$d = k\lambda / (\beta \cdot \cos\Theta)$$

where, d is the average particle size of biogenic nanoparticles, k is Scherrer constant, λ is X-ray wavelength, β is the width of the XRD pattern at half height and Θ is the Bragg diffraction angle.

The presence of functional groups in the synthesized iron oxide nanoparticles as a result of capping and stability provided by the phytochemicals was analyzed through Agilent Cary 630 FTIR. The biomolecules present in *A. indica* were adsorbed on the surface of biosynthesized nanoparticles. However, in order to prepare FeNPs samples, specimens were mixed with KBr powder at a 1% (w/w) ratio and the mixture was pressed into a sheer slice. The scanning electron microscope (SEM) was used to analyze the morphology of the obtained biogenic iron oxide-NPs. SEM images were acquired via (JSM5910, JEOL, Japan) scanning electron microscope at different magnifications. Transmission electron microscopy (TEM) and high-resolution transmission electron microscopy (HR-TEM) were used to determine the shape and particle size of nanoparticles. The elemental composition and crystallinity of biosynthesized nanoparticles were determined using energy dispersive X-ray spectroscopy (EDX) and selected area electron diffraction (SAED), respectively.

2.10.2. Activation of sodium persulphate using biosynthesized FeNPs for TPH degradation

Biosynthesized iron nanoparticles were utilized singly and synergistically with sodium persulphate for degradation of TPH. Experimental conditions for sodium persulphate activation were set at the optimum conditions which were achieved for TPH degradation using the oxidant and analyzed using response surface methodology; 0.74 M sodium persulphate at pH 6.0 within 5 days and 14 h. Sodium persulphate (0.74 M) was spiked with 0.07 and 0.15 g/L of AZA FeNP (2:1), respectively, and mixed with contaminated soil samples. 10 g of soil samples were withdrawn daily within this period and extraction of TPH was carried out using USEPA Method 8015D (USEPA, 2003). Analysis of TPH was carried out using Agilent 7890B gas chromatograph coupled with flame ionization detector (GC-FID).

3. Results and discussion

3.1. Preliminary screening

3.1.1. Physicochemical analysis of soil

Table 1 summarizes the results of the physicochemical analysis of the soil samples used in this study. According to the results, the soil texture had a high proportion of sand and coarse particles and would be classified as sandy soil according to the USDA textural triangle. Thus, the permeability of an oxidant/activator solution down the soil would be determined by the texture of the soil. More so, the MP-AES was also used to determine metal concentrations including calcium, copper, potassium, magnesium, nickel, lead, zinc, and iron.

Table 1
Physicochemical properties of the investigated soil samples.

| Parameter | Measured value |
|--------------------------------------|----------------|
| pH (soil: H ₂ O = 1: 2.5) | 7.80 ± 0.05 |
| Moisture content (%) | 0.20 ± 0.02 |
| Total organic carbon (%) | 0.14 ± 0.01 |
| Sand (%) | 68.33 |
| Silt (%) | 26.60 |
| Clay (%) | 5.07 |
| Calcium (mg/kg) | 6.63 ± 0.54 |
| Copper (mg/kg) | 0.57 ± 3.42 |
| Potassium (mg/kg) | 2.65 ± 0.35 |
| Magnesium(mg/kg) | 2.55 ± 0.70 |
| Iron (mg/kg) | 1.35 ± 0.75 |
| Nickel (mg/kg) | 0.13 ± 1.10 |
| Lead (mg/kg) | 0.32 ± 0.65 |
| Zinc (mg/kg) | 0.08 ± 10.74 |

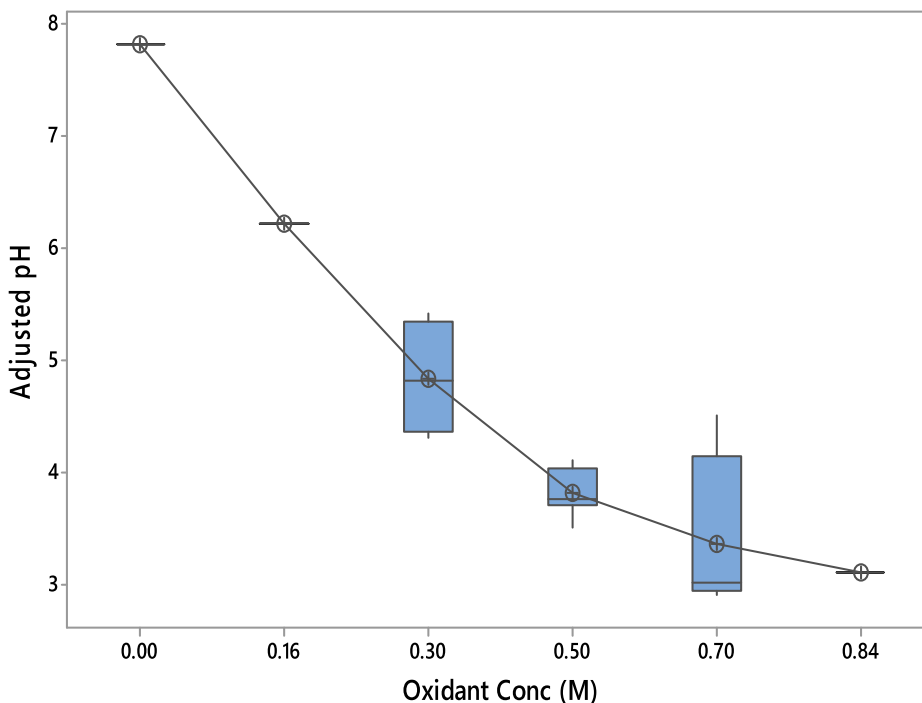


Fig. 2. Interval plot of adjusted pH vs oxidant concentration (M).

3.1.2. Effect of sodium persulphate dosage on pH of contaminated soil

The initial pH of petroleum-contaminated soil:oxidant mixture was observed to be 7.80. However, in order to achieve the experimental pH specified in the central composite design, pH adjustment was carried out using 0.1 M sodium hydroxide or 0.1 M hydrochloric acid, until the desired pH was achieved. The experimental condition for the degradation of TPH was designed to study the effect of oxidant dosage, pH and time on contaminated soil. The results obtained are presented in Table 3. The relationship between alkalinity of the mixture on addition of sodium persulphate is reported in Fig. 2. pH readings were taken in triplicates. The data is reported to 95% confidence interval for the mean. The pooled standard deviation was used to calculate intervals. The pH of the mixture changed in relation to oxidant dosage. The addition of 0.2 and 0.8 M sodium persulphate resulted in pH adjustment from 7.8 to 6.2 and 3.1, respectively. This indicates that the acidity of the soil–persulphate mixture increased with increasing persulphate concentration – prior to pH adjustment with sodium hydroxide or hydrochloric acid (Fig. 2).

Table 2
Design matrix and result of experiments for determination of TPH in contaminated soil.

| Std order | Run order | Pt type | Blocks | pH | Time (day) | Oxidant conc. | TPH soil |
|-----------|-----------|---------|--------|-----|------------|---------------|----------|
| 17 | 1 | 0 | 1 | 6.8 | 15.5 | 0.5 | 8641.4 |
| 12 | 2 | -1 | 1 | 6.8 | 29.8 | 0.5 | 2172.2 |
| 18 | 3 | 0 | 1 | 6.8 | 15.5 | 0.5 | 9920.9 |
| 6 | 4 | 1 | 1 | 7.5 | 7.0 | 0.7 | 754.3 |
| 8 | 5 | 1 | 1 | 7.5 | 24.0 | 0.7 | 1753.8 |
| 7 | 6 | 1 | 1 | 6.0 | 24.0 | 0.7 | 2511.5 |
| 20 | 7 | 0 | 1 | 6.8 | 15.5 | 0.5 | 7986.2 |
| 15 | 8 | 0 | 1 | 6.8 | 15.5 | 0.5 | 3546.6 |
| 11 | 9 | -1 | 1 | 6.8 | 1.2 | 0.5 | 6167.9 |
| 2 | 10 | 1 | 1 | 7.5 | 7.0 | 0.3 | 5653.5 |
| 3 | 11 | 1 | 1 | 6.0 | 24.0 | 0.3 | 794.4 |
| 5 | 12 | 1 | 1 | 6.0 | 7.0 | 0.7 | 1774.9 |
| 10 | 13 | -1 | 1 | 8.0 | 15.5 | 0.5 | 26.6 |
| 14 | 14 | -1 | 1 | 6.8 | 15.5 | 0.8 | 375.4 |
| 16 | 15 | 0 | 1 | 6.8 | 15.5 | 0.5 | 9909.2 |
| 9 | 16 | -1 | 1 | 5.5 | 15.5 | 0.5 | 545.3 |
| 19 | 17 | 0 | 1 | 6.8 | 15.5 | 0.5 | 6181.1 |
| 1 | 18 | 1 | 1 | 6.0 | 7.0 | 0.3 | 66.6 |
| 4 | 19 | 1 | 1 | 7.5 | 24.0 | 0.3 | 672.3 |
| 13 | 20 | -1 | 1 | 6.8 | 15.5 | 0.2 | 6867.2 |

3.2. Optimization studies

3.2.1. Central composite design experiments

One factor at three levels was tested to find the optimal extraction conditions for degradation of total petroleum hydrocarbons. For each experimental run, one variable was measured – TPH in soil (mg/kg). The design matrix and TPH value of each experimental run based on central composite design is presented in Table 2. Based on the central composite design, a model was generated and fitted to a quadratic polynomial model (Model S1). The *p* value for the model was 0.023 with correlation coefficient (R^2) of ~80%. The independent variables were all significant ($p < 0.05$), except for the models of two-way interactions.

At the center point of the design, six runs were made under the same conditions; 0.5 M sodium persulphate at pH 6.8 with reaction time of 15 days and 12 h. The TPH values obtained for these runs were 8641, 9921, 7986, 3547, 9909 and 6181 mg/kg (7968 ± 2249). Since the initial concentration of TPH was found to be 13,752.5 mg/kg, this represents the average degradation efficiency of ~40%. There were 8 cube points. The runs were made on day 7 and 24. On day 7, four runs were made at different conditions and the TPH values obtained were 754.3, 66.6, 5653.5 and 1774.9 mg/kg. On day 24, four runs were made with varying oxidant dosage and pH. The corresponding TPH values obtained were 1753.8, 2511.5, 794.4 and 672.3 mg/kg, respectively. The lowest and highest TPH concentration for runs carried out under these conditions were achieved on day 7 with 0.3 M sodium persulphate at pH of 6.0 and 7.5, respectively. There were 6 star points. The runs were all made on days 1.2, 15.5 and 29.8. The TPH value obtained for the first run on day 1.2 was 6,167.9 mg/kg. On day 15.5, four runs were made with varying oxidant dosage and pH. The results obtained are TPH values of 545.3, 6867.2, 375.4 and 26.6 mg/kg, respectively. The final run was made on day 29.8, with 2172.2 mg/kg of TPH obtained.

However, the mean TPH values obtained at days 7, 15.5 (star points) and 24, although conducted under varying conditions (pH and persulphate concentration), were 2062.3, 1653.6 and 1433.0 mg/kg, respectively. These values suggest that TPH concentration reduced with time. However, the average TPH values for samples analyzed at day 15.5; center and star points are at variance (7968 and 1654 mg/kg respectively), although the latter was conducted under varying conditions. Also, TPH concentration at 29.8 days was higher than the mean values obtained at days 7, 15.5 (star points) and 24, TPH concentration at the onset of degradation (day 1.2) was highest. From the results obtained, TPH degradation is not linear with respect to time alone but may likely be due to the combined effect of time, oxidant dosage and pH. Hence, response surface methodology was employed to predict the optimum condition for TPH degradation. The resulting contour plots are presented in Fig. 3a-c.

3.2.2. Analysis of response surfaces

The independent variable was found to have a significant effect on the concentration of TPH degraded in soil. Since this study aimed to maximize TPH degradation by achieving concentrations as low as possible, the optimal degradation conditions for achieving zero concentration based on the equation of the model were selected. TPH degradation was carried out over 30 days with 0.16 M–0.84 M sodium persulphate solution and pH ranging from 6 to 8 according to the experimental design. Analysis of the initial concentration of TPH in petroleum-contaminated soil was carried out and found to be 1.3753×10^4 mg/kg. The two-way interactions between any two conditions while holding the third constant are presented as contour plots (Fig. 3a–c). By keeping the concentration of sodium persulphate at 0.5 M, 5000–6500 mg/kg of TPH in soil was degraded at pH 6.0–7.5 within 25 days (Fig. 3a). Under these conditions less than 45% soil TPH was

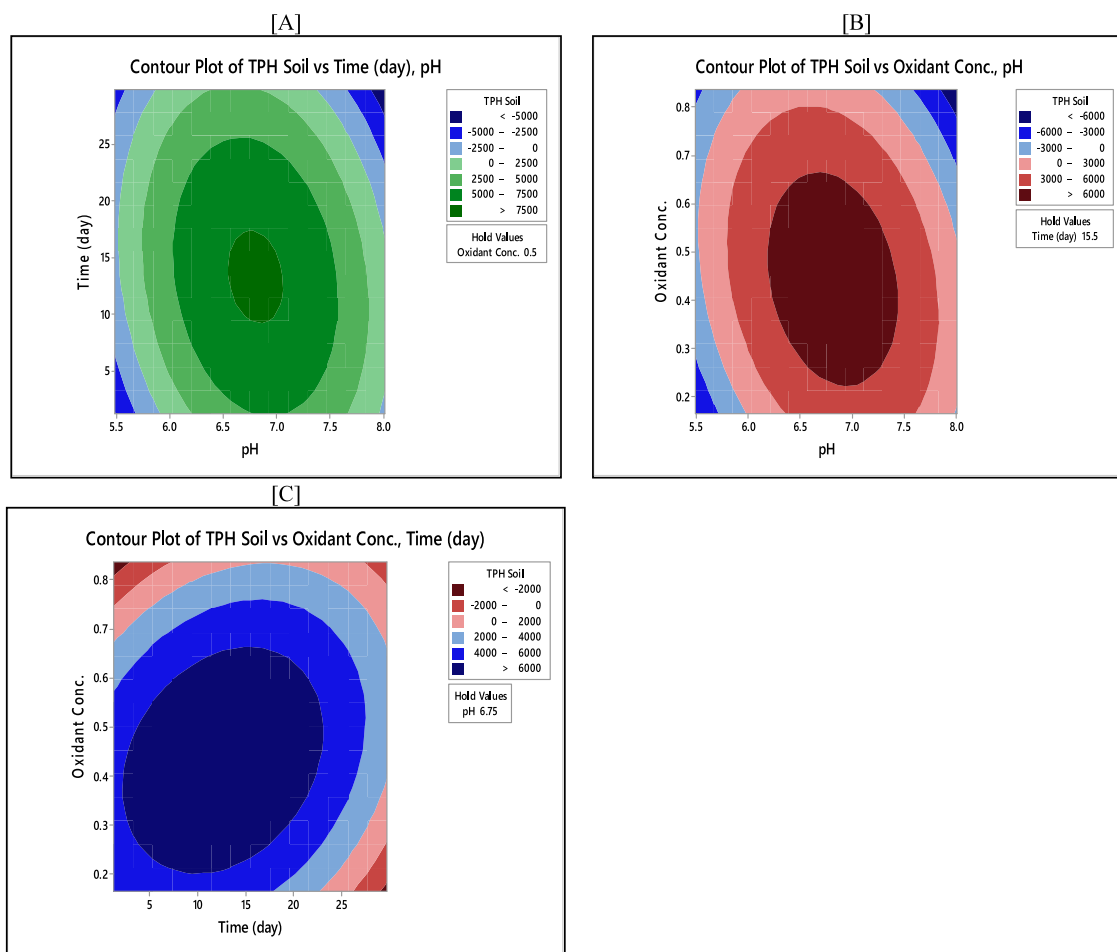


Fig. 3. a–c: Contour plots of TPH soil vs Time and pH [A], TPH soil vs persulphate concentration and pH [B], and TPH soil vs persulphate concentration and time [C].

degraded within 16 days. The relationship between oxidant concentration and pH can be explained using Fig. 3b. On day 15.5, about 7750 mg/kg of soil TPH was degraded at pH 6.2–7.4. To achieve this, 0.2–0.7 M sodium persulphate was required. Also, holding pH at 6.75 and varying dosage of sodium persulphate (0.16 M–0.65 M) within 20–25 days achieved about 50% degradation (Fig. 3c).

3.3. Degradation of TPH under optimized conditions


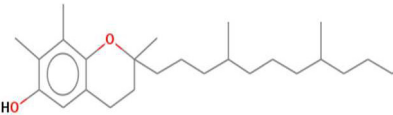
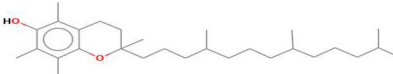
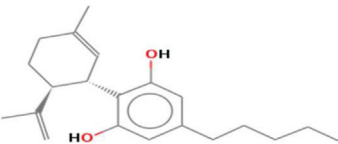
In order to achieve maximum degradation based on the model, optimum conditions were determined to be pH 6.9, oxidant concentration of 0.42 M within a period of 12.2 days. However, to achieve complete TPH degradation in soil, response predictions were pH 6.0 and oxidant concentration of 0.74 M within a period of 5.64 days. In order to verify the optimized conditions as determined by the RSM, response prediction to achieve complete degradation of soil TPH was chosen. New experiments were carried out at pH of 6.0, 0.74 M oxidant concentrations and several samples were withdrawn for analysis over 5.64 days (Fig. S1).

3.4. Synthesis and characterization of biogenic iron oxide nanoparticles

3.4.1. Preliminary GC-MS characterization of *A. indica* leaves

Due to its importance, *Azadirachta indica* has been declared the “Tree of the 21st Century” by the United Nations (Hossain et al., 2013). Ethanolic fraction of aqueous *A. indica* leaves extract was analyzed using GC-MS for the presence of phytochemicals, particularly polyphenols (Fig. S2). Phenols, organic acids, and carbohydrates were identified, amongst others. About 100 compounds were identified in total, out of which four were phenolic. Twelve compounds were present at 1% relative abundance or more. These compounds represent about 48% of the whole plant extract. Four phenolic

Table 3
Structural composition of phenolic constituents of *A. indica* leaf extract.

| RT | Area % | IUPAC name of compound | Mol. formular | Mol. weight | Chemical structure |
|------|--------|-------------------------|--|-------------|--|
| 13.7 | 0.259 | 2-Methoxy-4-vinylphenol | C ₉ H ₁₀ O ₂ | 150.175 |  |
| 36.5 | 0.183 | .gamma.-Tocopherol | C ₂₈ H ₄₈ O ₂ | 416.680 |  |
| 37.3 | 0.994 | Vitamin E | C ₂₉ H ₅₀ O ₂ | 430.706 |  |
| 41.9 | 0.669 | Cannabidiol | C ₂₁ H ₃₀ O ₂ | 314.462 |  |

constituents were identified in *A. indica*, representing 2.11% of the total phytochemicals in the ethanolic leaves extract (Table 3). Of these four, namely 2-methoxy-4-vinylphenol, gamma-tocopherol, vitamin E and cannabidiol, the latter two were the most abundant. A detailed description of constituents identified has been published in previous studies (Bolade et al., 2019b, 2018). Phytol (11.6%), 9,12,15-Octadecatrienoate (9.7%) and hexadecanoic acids (including their derivatives such as hexadecanoic acid ethyl ester) (9.4%) were the most abundant.

Previous studies on the GC–MS characterization of *A. indica* leaves have identified presence of phytochemicals such as phytol, linoleic acid, homo- γ -linoleic acid, palmitic acid and tridecanoic acid. These bioactive compounds have been known to contain antioxidant, antibacterial, anti-inflammatory and antidiuretic activities (Balasubramanian et al., 2019). Hexadecanoic acid was reported as one of the 12 components identified in aqueous extract of *A. indica* (Brindha and Mallika, 2015). According to Kamaraj et al. (2018), organic acids (hexadecanoic, oleic and linoleic acids) constitute about 50% of *A. indica* gum extract. Other constituents such as stearic acid ethyl ester and ricinoleic acid methyl ester were also identified. Phytochemical characterization of different extracts of *A. indica* (Omani neem) has also been reported by Hossain et al. (2013). N-alkanes, phenolic compounds, terpenoids, alkaloids and glycosides were identified. Previous studies carried out on the leaf, stem and root of *A. indica* sourced from Southwest Nigeria indicated the presence of twenty one compounds, including methyl ester and octadecanoic acid (Oshiobugie et al., 2017).

3.4.2. Reaction mixture and UV/Visible spectrophotometric analysis

Biosynthesis of iron nanoparticles was monitored using UV/Visible spectroscopy within a 250–500 nm wavelength range. *A. indica* leaf aqueous extract contains various phytochemicals, especially phenolic compounds that highly favored the formation of iron nanoparticles. *A. indica* aqueous extracts were mixed with ferric chloride in varying proportion, 1:1 and 2:1 to obtain brown precipitates labeled AZA FeNP (1:1) and AZA FeNP (2:1), respectively. The ferric chloride solution turned from yellowish to brown–black suspension as *A. indica* extract was added. The UV/Visible absorption spectrometric analysis revealed absorption spectrum at wavelength of ~ 300 nm, suggesting the bioreduction of ferric chloride to iron nanoparticles (Fig. S3). The result acquired was in absolute concurrence with previously published UV spectral analysis of metallic iron (Alam et al., 2018). The band gap energy, calculated using the equation ($E = hc/\lambda$ where h – plank's constant, c – velocity of light and λ – wavelength) is 3.27 eV. These data show the reduction of Fe³⁺ by *A. indica* leaf extract and stabilization of as-synthesized iron nanoparticles by the natural organic moieties such as polyphenols.

3.4.3. Fourier transform infrared spectroscopic (FTIR) analysis

FTIR spectroscopy was utilized to identify likely biomolecules responsible for the reduction of metal precursors and stabilization/capping of iron nanoparticles. The vibrational features of the biosynthesized nanoparticles were studied and the spectrum was recorded over the range 4000–650 cm⁻¹. The spectrum revealed the presence of moieties, which played a crucial role as stabilizing agents. The FTIR spectra obtained for concentrated aqueous *A. indica* extracts and iron oxide nanoparticles AZA FeNP (1:1) and AZA FeNP (2:1) show different absorption peaks, which represent various functional groups. The absorption peaks originated at around 1637, 1654 and 3319 cm⁻¹, respectively. The broad, strong band at 3300 cm⁻¹ is due to phenolic OH stretching vibration. The bands 1637 cm⁻¹ and 1654 cm⁻¹ can be associated with

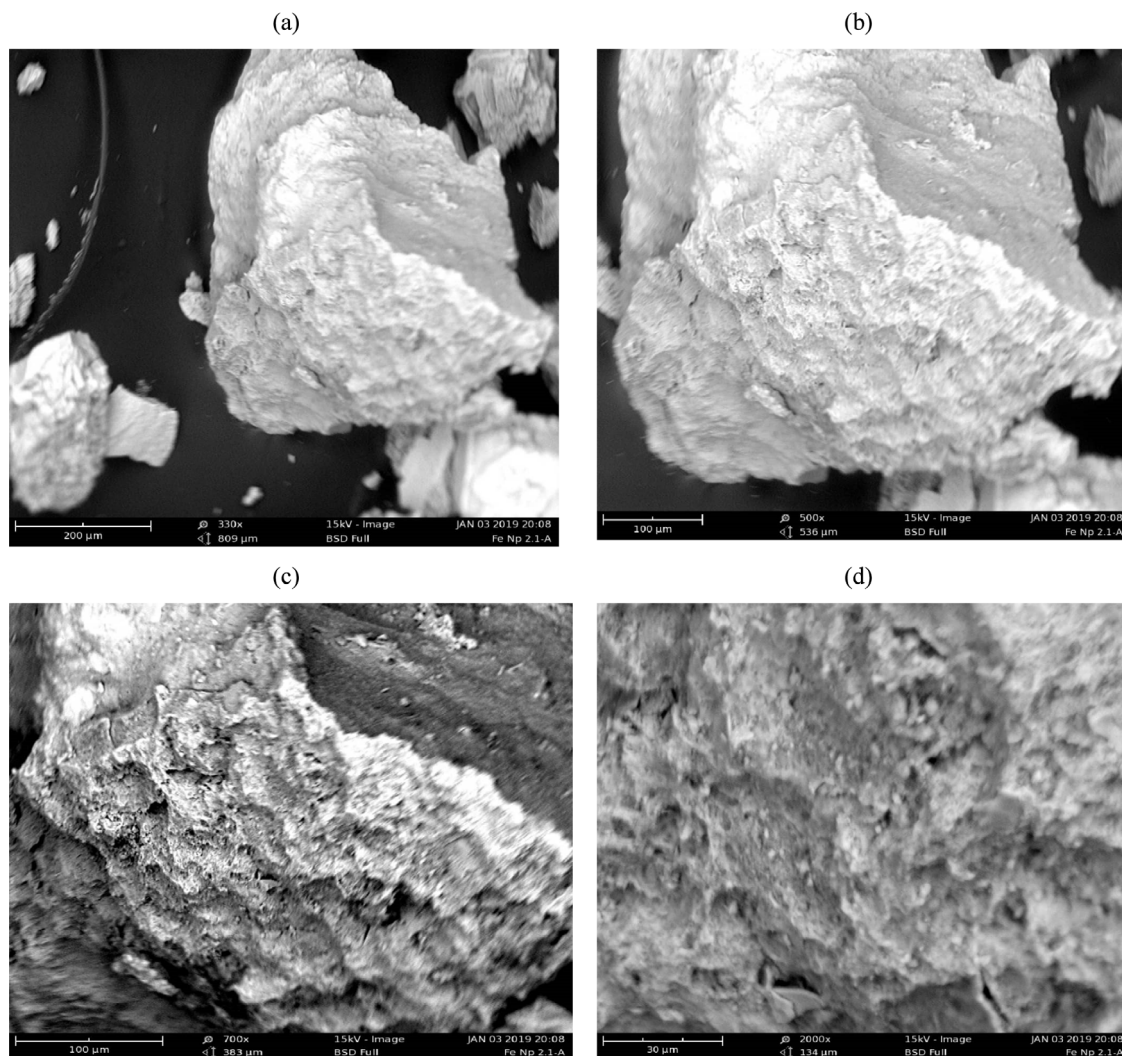


Fig. 4. SEM images of *A. indica* iron nanoparticles (FeNP AZA 1:1) showing different magnifications (a) $\times 330$ (b) $\times 500$ (c) $\times 700$ (d) $\times 2000$.

C=O stretch (carboxylic acid). The FeO-NPs were likely capped by vitamin E and cannabidiol biomolecules. The observed absorption bands in the FTIR spectra of *A. indica* extract and iron nanoparticles showed little change, indicating the likely involvement of plant biomolecules in the formation of iron nanoparticles. The slight shift in absorption band from 3319 cm^{-1} in the pure extract to 3306 cm^{-1} in iron nanoparticles might be due to the binding nature of the functional groups with metal precursor. These biomolecules remained adhered to biosynthesized iron nanoparticles surface despite being annealed at a temperature of $600\text{ }^{\circ}\text{C}$. A number of published research on FTIR spectra of nanoparticles synthesized using *A. indica* have highlighted that in comparison with FTIR spectra of aqueous plant extract, there was reduced intensity in the absorption band in nanoparticles spectra, which indicates that bioactive moieties present in the extract were involved in nanoparticles synthesis (Elumalai and Velmurugan, 2015; Singh and Kaushik, 2019).

3.4.4. X-ray diffraction (XRD) analysis

The XRD patterns of the biosynthesized nanoparticles are presented in Fig. S4. These provide phase information and the average size of the prepared nanoparticles. The broadened peaks and scattered X-ray lines indicated that biosynthesized AZA FeNPs were formed in the nanocrystalline regime. There appears to be deficiencies in the distinctive diffraction peaks, particularly in spectra of AZA FeNP (1:1) indicating that the synthesized Fe NPs were amorphous (Huang et al., 2015; Xiao et al., 2016). Furthermore, the XRD patterns exhibited two characteristic peaks at $2\theta = 35.4^{\circ}$, 44.5° , which can be attributed to iron oxide nanoparticles indicating the biogenic synthesis of nanoparticles and cubic texture (JCPDS Card no. 82-1533). The broad shoulder peak at around $2\theta = 27^{\circ}$ can be identified as organic components acting as capping agents. The narrower peaks for AZA FeNP (2:1) sample shows higher crystallinity than AZA FeNP (1:1) sample, which indicates

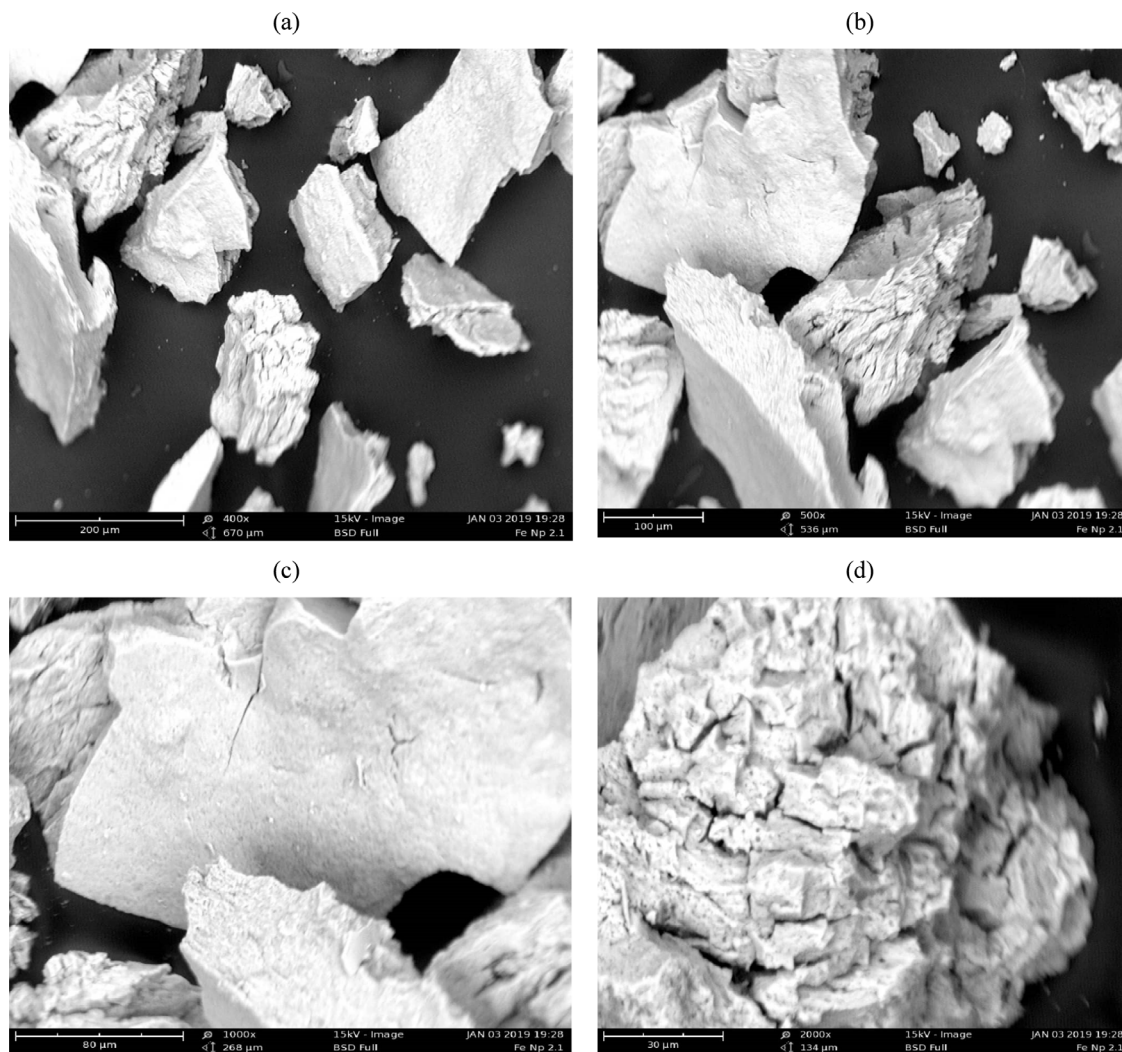


Fig. 5. EM images of *A. indica* iron nanoparticles (FeNP AZA 2:1) showing different magnifications (a) $\times 400$ (b) $\times 500$ (c) $\times 1000$ (d) $\times 2000$.

that the crystallinity increased with increase in the molar ratio concentration from 1:1 to 2:1. Similar results have been reported in previous studies (Liu et al., 2018; Madhubala and Kalaivani, 2018). The average crystallite size was evaluated using Debye–Scherrer equation. For AZA FeNP (2:1), the average crystallite size obtained using OriginPro 8.5 software is 1.2 nm. However, for AZA FeNP (1:1), using the most prominent peak for calculating the average crystallite size resulted in large error, with poor Gaussian distribution.

Scherrer equation:

$$D = K\lambda/d\cos\theta$$

where, D = crystallite size, $\lambda = 1.54060$ for Cukal, K = crystallite shape factor (~ 0.9), d = FWHM, and θ = angle (rad)

3.4.5. Scanning Electron Microscopy (SEM) analysis

Surface morphology of biosynthesized iron oxide nanoparticles was determined using SEM (Figs. 4 and 5). The images displayed agglomerated heterogeneous morphology, although there was decreased agglomeration in AZA FeNP (2:1), suggesting that heterogenous agglomeration decreased with increase in plant extract. This is possibly due to increased availability of capping and reducing agents. Similar studies have been reported for the synthesis of Fe_3O_4 @ZnO core-shell nanoparticles using *Azadirachta indica* extracts (Madhubala and Kalaivani, 2018). It has been reported that biosynthesized nanoparticles differ from those synthesized using chemical reducing agents such as sodium borohydride, which tend to have a more homogeneous size distribution (Chen et al., 2015). This is likely due to the differing reducing properties of bioactive constituents such as polyphenols found in *A. indica* aqueous extract. These phytochemicals expectedly play a crucial role in controlling size distribution and aggregation of nanoparticles via capping and stabilization.

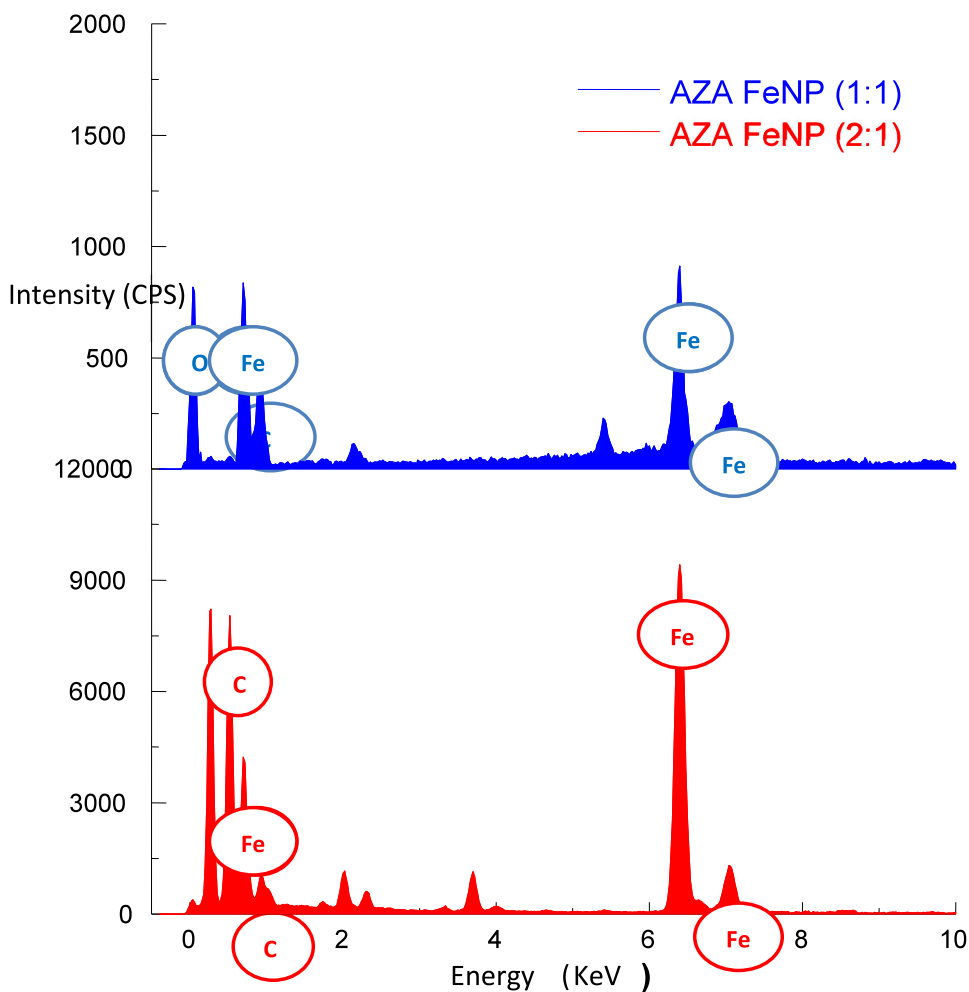


Fig. 6. EDX spectra of AZA FeNP (1:1) and AZA FeNP (2:1).

3.4.6. Energy Dispersive X-ray (EDX) Spectroscopic analysis

The energy dispersive X-ray spectroscopy (EDX) analysis was carried out (Fig. 6). The EDX spectrum of both AZA FeNP (1:1) and (2:1) displayed intense peaks of Fe, C and O, confirming the presence of iron. Oxygen, carbon and iron peaks at 0.4, 0.6 and 6.4 KeV were observed for AZA FeNP (1:1) and (2:1). The presence of Cu and C can be accounted for by using carbon- and copper-coated grids during sample preparation prior to EDX analysis. Gold, chromium, and copper impurities observed arose from the sample preparation procedure. The availability of oxygen and iron indicates the formation of iron and iron oxides nanoparticles. A previous study also established the presence of Fe and O peaks in the EDX analysis of biosynthesized iron nanoparticles using *A. indica* (Hassan et al., 2018).

3.4.7. Transmission electron microscopy (TEM) analysis

Further characterization of the morphology of biosynthesized iron oxide nanoparticles was studied using transmission electron microscopy (TEM) as indicated in Fig. 7. From the TEM analysis, the one-pot synthesis resulted in the formation of heterogeneous nanoparticles. For both AZA FeNP (1:1) and (2:1), iron nanoparticles appear to be spherical in shape. Agglomeration of nanoparticles was observed, which agrees with the result obtained from SEM analysis. The particle size of acquired AZA FeNP (1:1) and AZA FeNP (2:1) is 3–61 nm and 3–54 nm with average size obtained as ~9.3 nm and 10.0 nm, respectively. Histograms displaying particle size distribution of biosynthesized nanoparticles are presented in Fig. S5.

The presence of naturally occurring phytochemicals with different reducing properties found in aqueous extract of *A. indica* probably accounts for the size distribution of the iron nanoparticles. According to Gaumet et al. (2008), the size distribution and polydispersity index of nanoparticles is a function of different factors/conditions such as the refractive index of solvent, nature of dispersive medium, mean sizes of the nanoparticles and experimental methods employed.

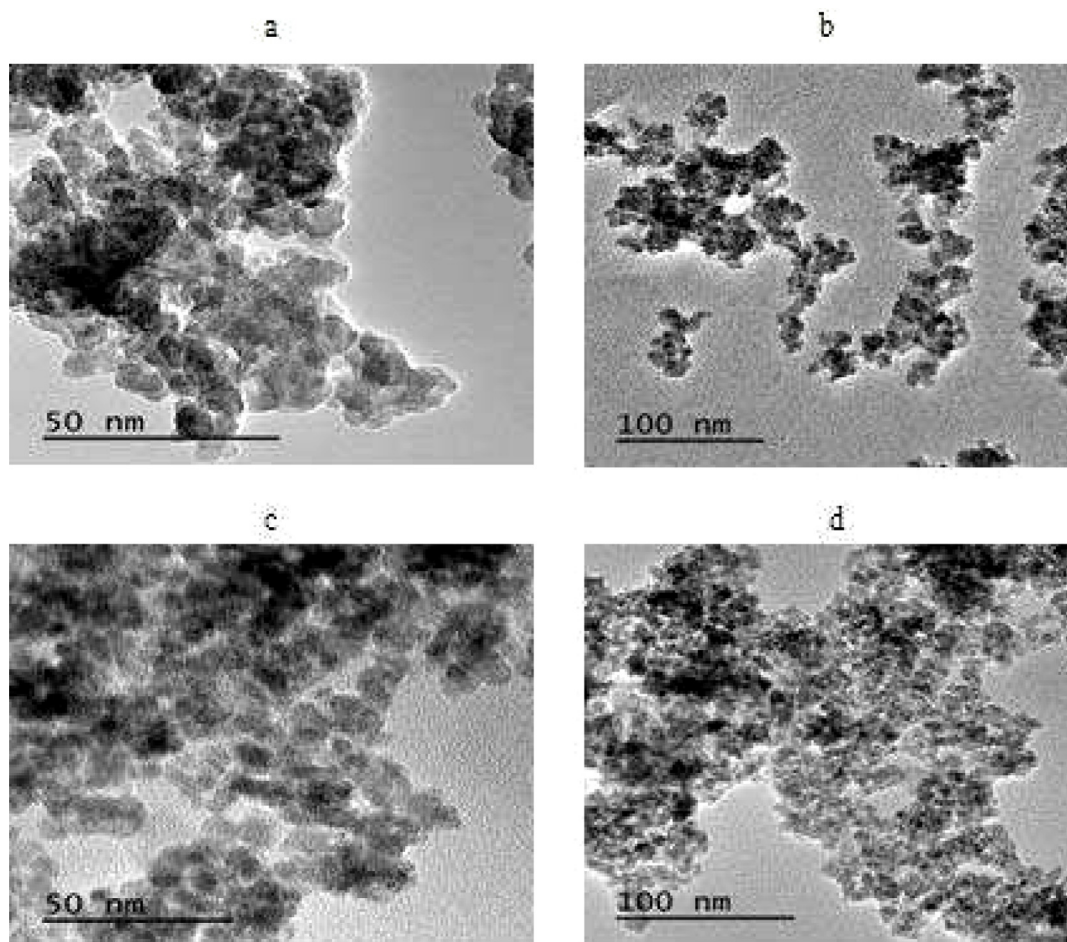
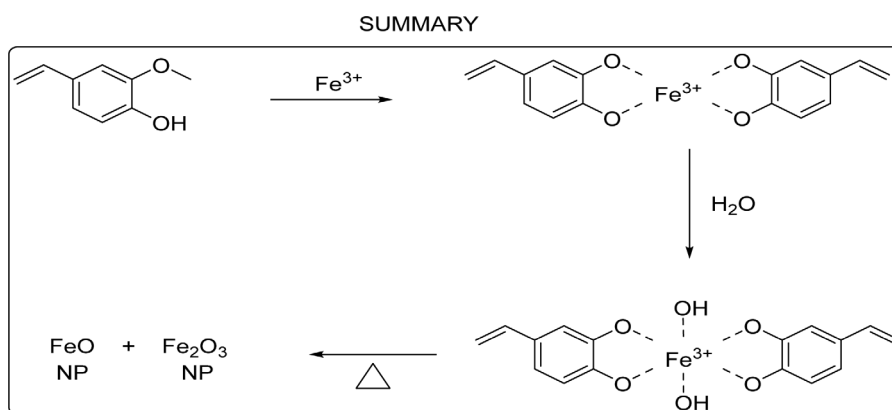


Fig. 7. TEM images of (a–b) AZA FeNP (1:1) (c–d) AZA FeNP (2:1).



3.4.8. High resolution transmission electron microscopy (HR-TEM) characterization

High resolution transmission electron microscopy (HR-TEM) analysis was carried out to further study nanoparticles shape and size distribution (Fig. 8). The HR-TEM images indicate that nanoparticles are spherical, with a pattern of more significant agglomeration in AZA FeNP (1:1). This agrees with the SEM images and XRD spectra, indicating the formation of nanoclusters resulting from the formation of amorphous nanoparticles. Nanoparticles agglomeration could have resulted from aqueous *A. indica* extracts during nanoparticles synthesis, which binds them together. It is also predicted that plant phytochemicals such as polyphenols may be coated over the iron nanoparticles, thereby reducing crystallinity. Previously, *A. indica* has been utilized for the synthesis of iron/iron oxide nanoparticles, and similar results were obtained (Hassan

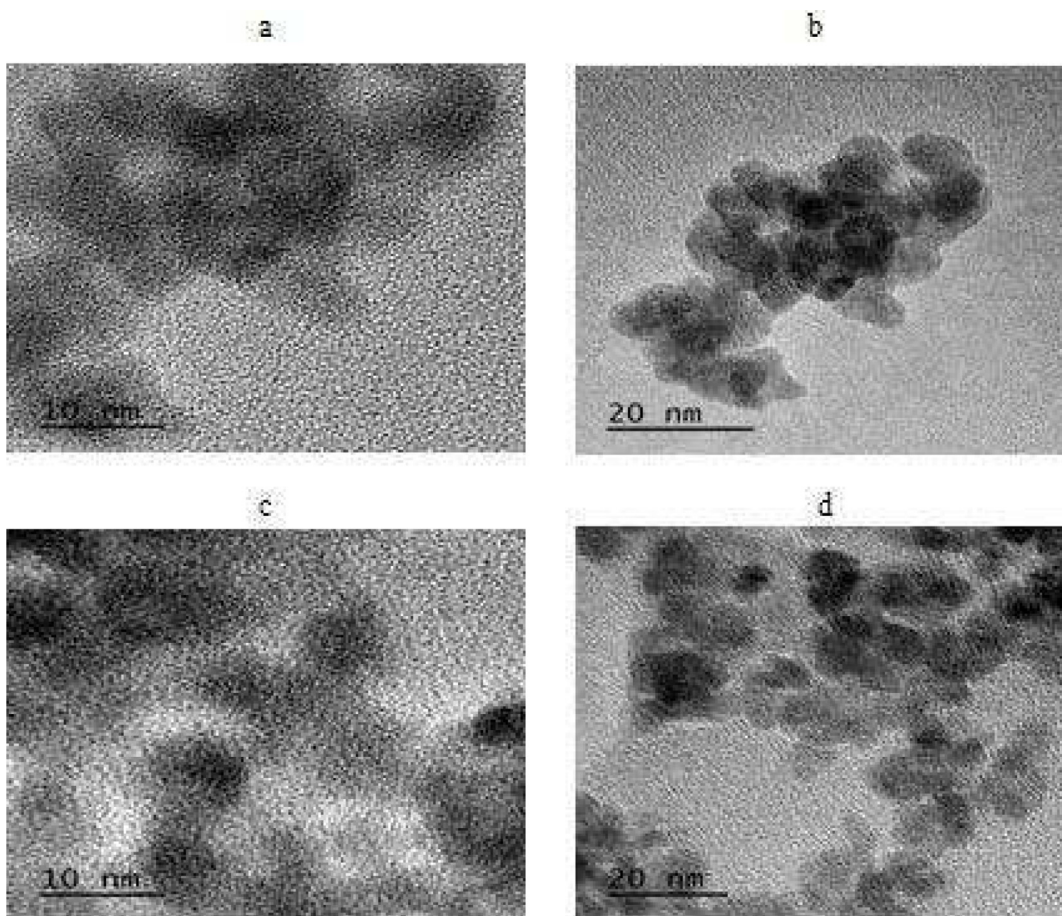


Fig. 8. HR-TEM images of (a–b) AZA FeNP (1:1) (c–d) AZA FeNP (2:1).

et al., 2018). Ebrahiminezhad et al. (2017) reported the synthesis of ultrasmall spherical iron nanoclusters using aqueous extract of Mediterranean cypress. Also, synthesis of $\text{Fe}_3\text{O}_4@\text{ZnO}$ core-shell nanoparticles using *A. indica* extracts has been reported (Madhubala and Kalaivani, 2018). The presence of phenolic compounds in the extracts likely contributed to the nanoparticles shape and size control by enhancing dispersion via surface capping.

3.4.9. Selected area electron diffraction (SAED) patterns

The crystallinity of iron oxide nanoparticles was tested using SAED (Fig. 9). The crystallinity can be deduced by the spotty ring pattern obtained by SAED. From the SAED, which was recorded from an area with large number of biogenic nanoparticles, it can be deduced that the nanoparticles are amorphous, although crystallinity increased slightly in AZA FeNP (2:1). This agrees with XRD patterns and SEM images of both nanoparticles.

3.5. Potential mechanism of nanoparticles synthesis

The reaction pathway for biosynthesis of nanoparticles is a function of several factors including the nature of extraction solvent, type of precursor used, pH, geographical location of plant sampling. Several studies have shown that different plants or plant parts contain varying composition of phytochemicals, which are likely reducing and stabilizing agents (Ali et al., 2016, 2019; Khatami et al., 2019; Karpagavinayagam and Vedhi, 2019; Lakshmi et al., 2019; Vasantharaj et al., 2019). Bioreduction, biostabilization and condensation are key stages in the synthesis process. During bioreduction, metal precursor such as ferric chloride is reduced by bioactive compounds in the plant extract. This process entails reduction of metal ions to a lower oxidation state owing to phytochemical reduction. Thereafter, agglomeration of ultrasmall nanoparticles into clusters and capping by phytochemicals to achieve morphological balance/stability occur. Using 2-methoxy-4-vinylphenol, a phenolic component of *A. indica* characterized using GC-MS in this study, we propose a likely reaction pathway for synthesis of iron oxide nanoparticles via aqueous extract and ferric chloride. This has been described further by Bolade et al. (2020) and Nasrollahzadeh et al. (2019).

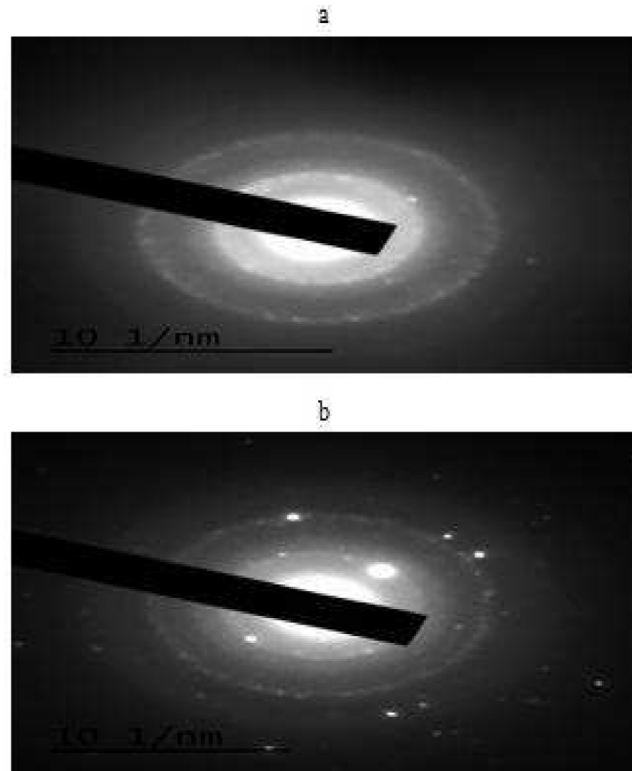


Fig. 9. Selected area electron diffraction pattern of (a) AZA FeNP (1:1) (b) AZA FeNP (2:1).

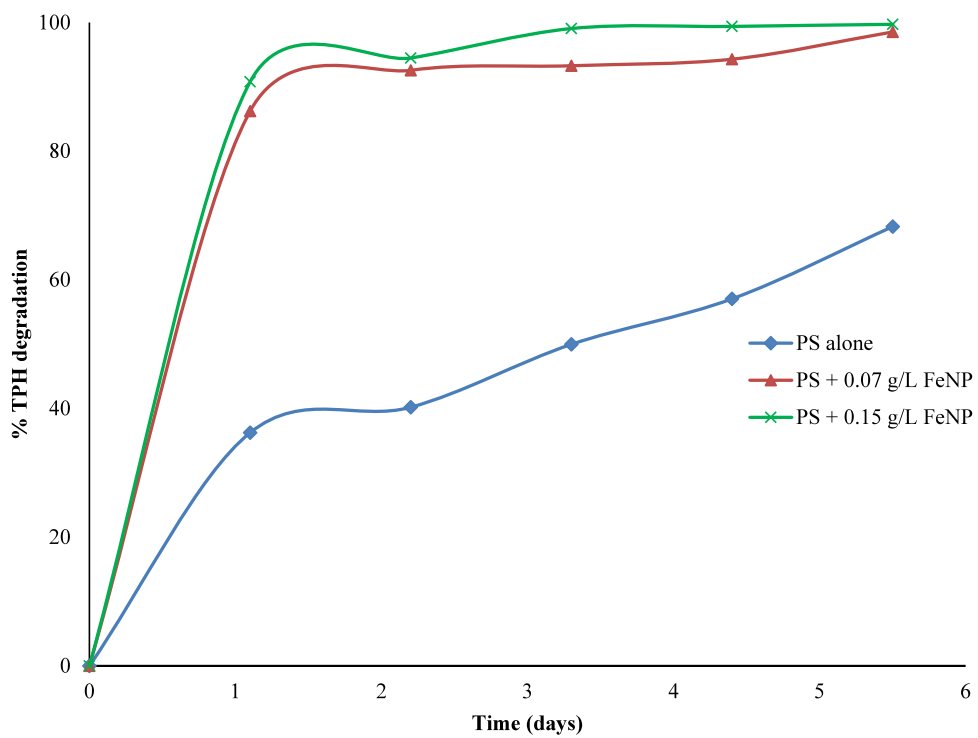


Fig. 10. Effect of nanoparticles-mediated persulphate activation on TPH degradation.

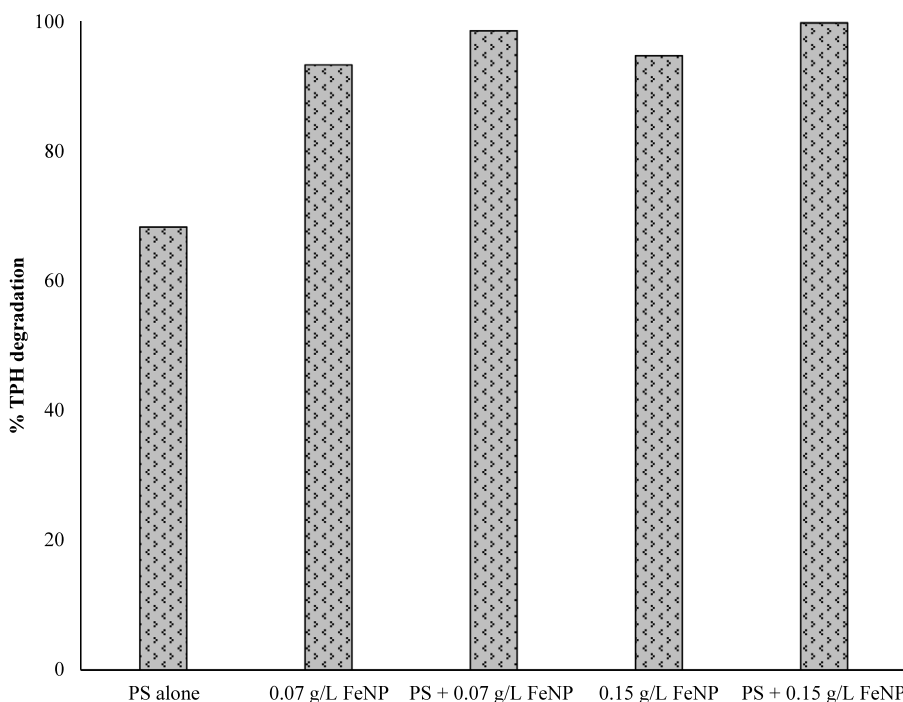


Fig. 11. Effect of synthesized nanoparticles (0.07 g/L and 0.15 g/L) and PS-FeNP (optimized) respectively on TPH degradation.

3.6. Catalyzed degradation of TPH with biogenic iron nanoparticles and sodium persulphate

The synergistic effect of biosynthesized iron nanoparticles (0.07 and 0.15 g/L) FeNP (2:1) and sodium persulphate for TPH degradation under optimized conditions (pH 6.0 and oxidant concentration 0.74 within 5 days 15 h) was studied (Fig. 10). As well as TPH degradation using only biosynthesized nanoparticles and unactivated sodium persulphate (Fig. 11). The initial concentration of TPH in contaminated soil (prior to degradation) was 1.3753×10^4 mg/kg. Using sodium persulphate alone, TPH concentration reduced linearly with increased time from $\sim 13,800$ mg/kg to 4400 mg/kg within 6 days. This represents about 68% TPH removal under optimized conditions. Biosynthesized nanoparticles alone achieved better degradation efficiency than unactivated sodium persulphate. With 0.07 and 0.15 g/L FeNP (2:1), TPH concentration reduced to 928 and 732 mg/kg, respectively. This represents ~ 93 and 94% TPH degradation, respectively. Catalyzed degradation of TPH using FeNP (2:1)-activated sodium persulphate achieved near-complete degradation. Using sodium persulphate activated with 0.07 g/L FeNP (2:1), 86% TPH degradation was achieved within the first 27 h. This is significantly higher than TPH degradation using unactivated sodium persulphate within the same period. After 5 days 12 h, TPH concentration reduced to 203 mg/kg, representing $\sim 99\%$ degradation. Similarly, sodium persulphate activated with 0.15 g/L FeNP (2:1) achieved near-complete TPH degradation (99.7%) within the study period of 5 days 14 h. However, sodium persulphate activated with 0.15 g/L achieved 99% TPH degradation in about three-fifth the time it took sodium persulphate activated with 0.07 g/L i.e., within 3 days 8 h. Thus, TPH concentration decreased from $\sim 13,800$ to 131 mg/kg using the latter. This implies that the rate of activation is dependent on dosage/concentration of nanoparticles.

In separate studies, Desalegn et al. (2018) and Usman et al. (2018) investigated the degradation of TPH in petroleum-contaminated sediments using iron nanoparticles and sodium persulphate. Both achieved improved degradation efficiency with activated persulphate. This can be attributed to the very strong radicals produced when ferric iron reacts with sodium persulphate. Usman et al. (2012) also reported the efficiency of magnetite catalyzed sodium persulphate for oxidative degradation of refractory hydrocarbons including n-alkanes. Greater than 80% degradation of hydrocarbons in soil contaminated with fresh crude oil and weathered oil was achieved within one week at circumneutral pH. In contrast, soluble iron II ions (in place of magnetite), only achieved 10%–15% hydrocarbon degradation.

4. Conclusions

The study successfully optimized the degradation of total petroleum hydrocarbons in contaminated soil using sodium persulphate as oxidant. The optimum condition for complete degradation of total petroleum hydrocarbons was determined to be pH 6.0 and oxidant dosage 0.74 M within 5 days and 14 h. Bioactive constituents (which can act as reducing and stabilizing agents during nanoparticles synthesis) from *Azadirachta indica* – a locally sourced plants were

characterized. Synthesis and characterization of iron nanoparticles using *A. indica* were successfully carried out. Spherical, amorphous iron oxide nanoparticles with a particle size distribution of ~9 and 10 nm were synthesized and characterized using UV/VIS, FTIR, SEM, XRD, TEM, HR-TEM, EDX and SAED. Biosynthesized iron nanoparticles (FeNP (2:1)) were applied for degradation of TPH in soil and activation of sodium persulphate for the same purpose. Nanoparticles-activated persulphate successfully degraded ~99% TPH in soil within 5 days 14 h.

CRediT authorship contribution statement

Oladotun P. Bolade: Conceptualization, Data curation, Formal analysis, Investigation, Methodology, Writing - original draft, Writing - review & editing. **Anuoluwa A. Akinsiku:** Formal analysis, Investigation, Writing - review & editing. **Oluwatobi S. Oluwafemi:** Data curation, Formal analysis, Writing - review & editing. **Akan B. Williams:** Conceptualization, Investigation, Supervision, Writing - review & editing. **Nsikak U. Benson:** Conceptualization, Data curation, Funding acquisition, Investigation, Methodology, Project administration, Supervision, Writing - review & editing.

Declaration of competing interest

The authors declare that they have no known competing financial interests or personal relationships that could have appeared to influence the work reported in this paper.

Acknowledgments

This research was supported by the Covenant University Center for Research, Innovation and Discovery (CUCRID), Nigeria, through the Covenant University Seed Grant. The authors are grateful to Covenant University for providing publication assistance.

Appendix A. Supplementary data

Supplementary material related to this article can be found online at <https://doi.org/10.1016/j.eti.2021.101719>.

References

- Abdullah, J.A., Eddine, L.S., Abderrhmane, B., Alonso-González, M., Guerrero, A., Romero, A., 2020. Green synthesis and characterization of iron oxide nanoparticles by pheonix dactylifera leaf extract and evaluation of their antioxidant activity. *Sustain. Chem. Pharm.* 17, 100280, <https://doi.org/10.1016/j.scp.2020.100280>.
- Aceró, J.L., Benítez, F.J., Real, F.J., Rodríguez, E., 2018. Degradation of selected emerging contaminants by UV-activated persulfate : kinetics and influence of matrix constituents. *Sep. Purif. Technol.* <https://doi.org/10.1016/j.seppur.2018.02.055>.
- Alam, T., Asad, R., Khan, A., Ali, A., Sher, H., Ali, M., 2018. Biogenic synthesis of iron oxide nanoparticles via *skimmia laureola* and their antibacterial efficacy against bacterial wilt pathogen *Ralstonia solanacearum*. *Mater. Sci. Eng. C* <https://doi.org/10.1016/j.msec.2018.12.117>.
- Ali, K., Ahmed, B., Ansari, S.M., Saquib, Q., Al-khedhairi, A.A., 2019. Comparative in situ ROS mediated killing of bacteria with bulk analogue, Eucalyptus leaf extract (ELE) -capped and bare surface copper oxide nanoparticles. *Mater. Sci. Eng. C* 100 (2018), 747–758, <https://doi.org/10.1016/j.msec.2019.03.012>.
- Ali, K., Dwivedi, S., Azam, A., Saquib, Q., Al-said, M.S., Alkhedhairi, A.A., Musarrat, J., 2016. Aloe vera extract functionalized zinc oxide nanoparticles as nanoantibiotics against multi-drug resistant clinical bacterial isolates. *J. Colloid Interface Sci.* 472, 145–156, <https://doi.org/10.1016/j.jcis.2016.03.021>.
- American Society for Testing and Materials (ASTM) D2974-00, 2000. Standard Test Methods for Moisture, Ash, and Organic Matter of Peat and Other Organic Soils. ASTM, International, West Conshohocken, PA, www.astm.org.
- Anastas, P.T., Warner, J.C., 1998. *Green Chemistry: Theory and Practice*. Oxford University Press, New York, pp. 29–56.
- Ashworth, J., Keyes, D., Kirk, R., Lessard, R., 2001. Standard procedure in the hydrometer method for particle size analysis. *Commun. Soil Sci. Plant Anal.* 32 (5–6), 633–634, <http://dx.doi.org/10.1081/CSS-100103897>.
- Balasubramanian, S., Ganesh, D., Narayana, S., 2019. GC-MS analysis of phytochemicals in the methanolic extract of *Azadirachta*. *Int. J. Pharma Biosci.* 5 (4), 258–262.
- Bhuiyan, Md.S.H., Miah, M.Y., Paul, S.C., Aka, T.D., Saha, O., Rahaman, Md.M., Sharif, Md.J.I., Habiba, O., Ashaduzzaman, Md., 2020. Green synthesis of iron oxide nanoparticle using *Carica papaya* leaf extract: application for photocatalytic degradation of remazol yellow RR dye and antibacterial activity. *Heliyon* 6 (8), e04603, <https://doi.org/10.1016/j.heliyon.2020.e04603>.
- Biswas, A., Vanlalveni, C., Lalfakzuala, R., Nath, S., Rokhum, L., 2021. *Mikania mikrantha* leaf extract mediated biogenic synthesis of magnetic iron oxide nanoparticles: Characterization and its antimicrobial activity study. *Mater. Today Proc.* 42 (Part 2), 2214, 1366-1373-7853, <https://doi.org/10.1016/j.matpr.2021.01.108>.
- Bolade, O.P., Adeniyi, K.O., Williams, A.B., Benson, N.U., 2021. Remediation and optimization of petroleum hydrocarbons degradation in contaminated water using alkaline activated persulphate. *J. Environ. Chem. Eng.* 9 (4), 105801, <https://doi.org/10.1016/j.jece.2021.105801>.
- Bolade, O.P., Akinsiku, A.A., Adeyemi, A.O., Jolayemi, G.E., Williams, A.B., Benson, N.U., 2019b. Qualitative analysis, total phenolic content, FT-IR and GC-MS characterisation of *Canna indica*: bioreducing agent for nanoparticles synthesis. *J. Phys.: Conf. Ser.* 1299, 012135, <http://dx.doi.org/10.1088/1742-6596/1299/1/012135>.
- Bolade, O.P., Akinsiku, A.A., Adeyemi, A.O., Williams, A.B., Benson, N.U., 2018. Dataset on phytochemical screening, FTIR and GC-MS characterisation of *Azadirachta indica* and *Cymbopogon citratus* as reducing and stabilising agents for nanoparticles synthesis. *Data in Brief* 20, 917–926, <https://doi.org/10.1016/j.dib.2018.08.133>.
- Bolade, O.P., Durodola, B.M., Williams, A.B., Benson, N.U., 2019a. Persulphate-based degradation of total petroleum hydrocarbons in contaminated water. *J. Phys. Conf. Ser.* 1378 (Part 2), 032050, <https://doi.org/10.1088/1742-6596/1378/3/032050>.

- Bolade, O.P., Williams, A.B., Benson, N.U., 2020. Green synthesis of iron-based nanomaterials for environmental remediation: A review. *Environ. Nanotechnol. Monit. Manage.* 13, 100279, <https://doi.org/10.1016/j.enmm.2019.100279>.
- Brindha, T., Mallika, J., 2015. GC-MS analysis of naturally occurring gum exudates of *Azadirachta indica* A. Juss. *Int. J. Pharm. Chem.* 05 (06), 227–231, <https://doi.org/10.7439/ijpc>.
- Chen, F., Xie, S., Huang, X., Qiu, X., 2015. Ionothermal synthesis of Fe₃O₄ magnetic nanoparticles as efficient heterogeneous fenton-like catalysts for degradation of organic pollutants with H₂O₂. *J. Hard Mater.* 322, 152–162, <https://doi.org/10.1016/j.jhazmat.2016.02.073>.
- Contreras-calderón, J., Calderón-jaimés, L., Guerra-hernández, E., García-villanova, B., 2011. Antioxidant capacity, phenolic content and vitamin C in pulp, peel and seed from 24 exotic fruits from Colombia. *Food Res. Int.* 44 (7), 2047–2053, <https://doi.org/10.1016/j.foodres.2010.11.003>.
- Da Silva, C.K.O., Vianna, M.M.G.R., Foletto, E.L., Chivone-Filho, O., Do Nascimento, C.A.O., 2015. Optimizing phenanthrene and anthracene oxidation by sodium persulfate and Fe-modified diatomite using the response surface method. *Water Air Soil Pollut.* 226 (4), <https://doi.org/10.1007/s11270-015-2362-1>.
- Desalegn, B., Megharaj, M., Chen, Z., Naidu, R., 2018. Green mango peel-nanozerovalent iron activated persulfate oxidation of petroleum hydrocarbons in oil sludge contaminated soil. *Environ. Technol. Innov.* 11, 142–152, <https://doi.org/10.1016/j.eti.2018.05.007>.
- Ebrahimezhad, A., Taghizadeh, S., Ghasemi, Y., Berenjian, A., 2017. Green synthesized nanoclusters of ultra-small zero valent iron nanoparticles as a novel dye removing material. *Sci. Total Environ.* <https://doi.org/10.1016/j.scitotenv.2017.10.076>.
- Elumalai, K., Velmurugan, S., 2015. Green synthesis, characterization and antimicrobial activities of zinc oxide nanoparticles from the leaf extract of *Azadirachta indica* (L.). *Appl. Surf. Sci.* 345, 329–336, <https://doi.org/10.1016/j.apsusc.2015.03.176>.
- Gaumet, M., Vargas, A., Gurny, R., Delie, F., 2008. Nanoparticles for drug delivery: The need for precision in reporting particle size parameters. *Eur. J. Pharmaceut. Biopharmaceut.* 69 (1), 1–9, <https://doi.org/10.1016/j.ejpb.2007.08.001>.
- Hassan, D., Khalil, A.T., Saleem, J., Diallo, A., Shinwari, Z.K., Maaza, M., Hassan, D., Khalil, A.T., Saleem, J., Diallo, A., 2018. Biosynthesis of pure hematite phase magnetic iron oxide nanoparticles using floral extracts of *Callistemon viminalis* (bottlebrush): their physical properties and novel biological applications. *Artif. Cells Nanomed. Biotechnol.* 46 (S1), S693–S707, <https://doi.org/10.1080/21691401.2018.1434534>.
- Hossain, M.A., Al-toubi, W.A.S., Welji, A.M., Al-riyami, Q.A., Al-sabahi, J.N., 2013. Identification and characterization of chemical compounds in different crude extracts from leaves of Omani neem. *Integr. Med. Res.* 7 (4), 181–188, <https://doi.org/10.1016/j.jtusci.2013.05.003>.
- Huang, L., Luo, F., Chen, Z., Megharaj, M., Naidu, R., 2015. Green synthesised conditions impacting on the reactivity of FeNPs for the degradation of malachite green. *Spectrochim. Acta A* 137, 154–159, <https://doi.org/10.1016/j.saa.2014.08.116>.
- Jagathesan, G., Rajiv, P., 2018. Biosynthesis and characterization of iron oxide nanoparticles using *Eichhornia crassipes* leaf extract and assessing their antibacterial activity. *Biocatal. Agric. Biotechnol.* 13, 90–94, <https://doi.org/10.1016/j.bcab.2017.11.014>.
- Jiemvarangkul, P., Zhang, W., Lien, H., 2011. Enhanced transport of polyelectrolyte stabilized nanoscale zero-valent iron (nZVI) in porous media. *Chem. Eng. J.* 170 (2–3), 482–491, <https://doi.org/10.1016/j.cej.2011.02.065>.
- Kamaraj, C., Rajiv, P., Elango, G., 2018. Novel and environmental friendly approach; Impact of Neem (*Azadirachta indica*) gum nano formulation (NGNF) on *Helicoverpa armigera* (Hub.) and *Spodoptera litura* (Fab.). *Int. J. Biol. Macromol.* 107, 59–69, <https://doi.org/10.1016/j.ijbiomac.2017.08.145>.
- Karpagavinayagam, P., Vedhi, C., 2019. Green synthesis of iron oxide nanoparticles using *Avicennia marina* flower extract. *Vacuum* 160 (12159), 286–292, <https://doi.org/10.1016/j.vacuum.2018.11.043>.
- Khatami, M., Alijani, H.Q., Fakheri, B., Mobasser, M.M., Heydarpour, M., Farahani, Z.K., Ullah, A., 2019. Super-paramagnetic iron oxide nanoparticles (SPIOs): Greener synthesis using stevia plant and evaluation of its antioxidant properties. *J. Cleaner Prod.* 208, 1171–1177, <https://doi.org/10.1016/j.jclepro.2018.10.182>.
- Kirdat, P.N., Dandge, P.B., Hagwane, R.M., Nikam, A.S., Mahadik, S.P., Jirange, S.T., 2021. Synthesis and characterization of ginger (*Z. officinale*) extract mediated iron oxide nanoparticles and its antibacterial activity. *Mater. Today: Proc.* 43 (Part 4), 2826–2831, <https://doi.org/10.1016/j.matpr.2020.11.422>.
- Kurowska-Susdorf, A., Zwierzdyński, M., Bevanda, A.M., Talić, S., Ivanković, A., Plotka-Wasyłka, J., 2019. Green analytical chemistry: social dimension and teaching. *TrAC - Trends Anal. Chem.* 111, 185–196, <https://doi.org/10.1016/j.trac.2018.10.022>.
- Lakshmi, P.P., Krishna, M.G., Venkateswara, R.K., Shanker, K., 2019. Biosynthesis, characterization and acute oral toxicity studies of synthesized iron oxide nanoparticles using ethanolic extract of centella asiatica plant. *Mater. Lett.* 236, 256–259, <https://doi.org/10.1016/j.matlet.2018.10.037>.
- Lemaire, J., Bues, M., Kabeche, T., Hanna, K., Simonnot, M., 2013a. Oxidant selection to treat an aged PAH contaminated soil by in situ chemical oxidation. *J. Environ. Chem. Eng.* 1, 1261–1268, <https://doi.org/10.1016/j.jece.2013.09.018>.
- Lemaire, J., Laurent, F., Leyval, C., Schwartz, C., Buès, M., Simonnot, M., 2013b. PAH oxidation in aged and spiked soils investigated by column experiments. *Chemosphere* 91 (3), 406–414, <https://doi.org/10.1016/j.chemosphere.2012.12.003>.
- Li, J., Li, Y., Wu, H., Naraginti, S., Wu, Y., 2021. Facile synthesis of ZnO nanoparticles by *Actinidia deliciosa* fruit peel extract: Bactericidal, anticancer and detoxification properties. *Environ. Res.* 111433, <https://doi.org/10.1016/j.envres.2021.111433>.
- Liu, Y., Jin, X., Chen, Z., 2018. The formation of iron nanoparticles by eucalyptus leaf extract and used to remove Cr (VI). *Sci. Total Environ.* 627, 470–479, <https://doi.org/10.1016/j.scitotenv.2018.01.241>.
- Madhubala, V., Kalaivani, T., 2018. Phyto and hydrothermal synthesis of Fe₃O₄@ZnO core-shell nanoparticles using *Azadirachta indica* and its cytotoxicity studies. *Appl. Surf. Sci.* 449, 584–590, <https://doi.org/10.1016/j.apsusc.2017.12.105>.
- Majidi, S., Zeinali Sehrg, F., Farkhani, S.M., Soleymani Goloujeh, M., Akbarzadeh, A., 2016. Current methods for synthesis of magnetic nanoparticles. *Artif. Cells Nanomed. Biotechnol.* 44 (2), 722–734, <https://doi.org/10.3109/21691401.2014.982802>.
- Matzek, L.W., Carter, K.E., 2016. Activated persulfate for organic chemical degradation: A review. *Chemosphere* 151, 178–188, <https://doi.org/10.1016/j.chemosphere.2016.02.055>.
- Naraginti, S., Li, Y., 2017. Preliminary investigation of catalytic, antioxidant, anticancer and bactericidal activity of green synthesized silver and gold nanoparticles using *Actinidia deliciosa*. *J. Photochem. Photobiol. B* 170, 225–234.
- Nasrollahzadeh, M., Atarod, M., Sajjadi, M., 2019. Plant-mediated green synthesis of nanostructures: Mechanisms, characterization, and applications. In: *An Introduction To Green Nanotechnology*, 1st ed. Elsevier Ltd., p. 28, <https://doi.org/10.1016/b978-0-12-813586-0.00006-7>.
- Okuo, J., Emina, A., Omorogbe, S., Anegebe, B., 2018. Synthesis, characterization and application of starch stabilized zerovalent iron nanoparticles in the remediation of Pb-acid battery soil. *Environ. Nanotechnol. Monit. Manage.* 9 (2017), 12–17, <https://doi.org/10.1016/j.enmm.2017.11.004>.
- Oshibugie, M.J., Olaniyi, A.M., Raphael, A.O., 2017. AAS And GC-MS analysis of phytochemicals in the leaf, stem and root of *Azadirachta indica*. *Br. J. Pharm. Res.* 15 (4), 1–12, <https://doi.org/10.9734/BJPR/2017/30611>.
- Patay, B., Sali, N., Csepregi, R., Bal, L., N, Tibor, N., 2016. Antioxidant potential, tannin and polyphenol contents of seed and pericarp of three coffee species. *Asian Pac. J. Trop. Med.* 9 (4), 366–371, <https://doi.org/10.1016/j.apjtm.2016.03.014>.
- Perveen, R., Shujaat, S., Qureshi, Z., Nawaz, S., Khan, M.I., Iqbal, I., 2020. Green versus sol-gel synthesis of ZnO nanoparticles and antimicrobial activity evaluation against panel of pathogens. *J. Mater. Res. Technol.* 9, 7817–7827.
- Prabhakar, R., Samadder, S.R., 2017. Aquatic and terrestrial weed mediated synthesis of iron nanoparticles for possible application in wastewater remediation. *J. Cleaner Prod.* 168, 1201–1210, <https://doi.org/10.1016/j.jclepro.2017.09.063>.
- Rafael, Á.C., Victor Irahuen, G.P., Marco Antonio, Á.P., Jesús Ángel, A.A., 2021. Green synthesis of ZnO nanoparticles using a *Dysphania ambrosioides* extract. *Struct. Character. Antibacterial propert.. Mater. Sci. Eng.* 118, 111540.

- Patiño Ruiz, D., Sánchez-Botero, L., Tejada-Benitez, L., Hinestroza, J., Herrera, A., 2020. Green synthesis of iron oxide nanoparticles using *cymbopogon citratus* extract and sodium carbonate salt: Nanotoxicological considerations for potential environmental applications. *Environ. Nanotechnol. Monit. Manage.* 14, 100377, <https://doi.org/10.1016/j.enmm.2020.100377>.
- Sam, K., Coulon, F., Prpich, G., 2017. Management of petroleum hydrocarbon contaminated sites in Nigeria: Current challenges and future direction. *Land Use Policy* 64, 133–144, <https://doi.org/10.1016/j.landusepol.2017.01.051>.
- Sathya, K., Saravanathamizhan, R., Baskar, G., 2017. Ultrasound assisted phytosynthesis of iron oxide nanoparticle. *Ultrasonics - Sonochem.* 39, 446–451, <https://doi.org/10.1016/j.ultsonch.2017.05.017>.
- Singh, K., Chopra, D.S., Singh, D., Singh, N., 2020. Optimization and ecofriendly synthesis of iron oxide nanoparticles as potential antioxidant. *Arab. J. Chem.* 13, 9034–9046, <https://doi.org/10.1016/j.arabjc.2020.10.025>.
- Singh, A., Kaushik, M., 2019. Physicochemical investigations of zinc oxide nanoparticles synthesized from *Azadirachta indica* (Neem) leaf extract and their interaction with calf-thymus DNA. *Results Phys.* 102168, <https://doi.org/10.1016/j.rinp.2019.102168>.
- Sun, M., Cheng, G., Ge, X., Chen, M., Wang, C., Lou, L., Xu, X., 2018. Environment aqueous Hg (II) immobilization by chitosan stabilized magnetic iron sulfide nanoparticles. *Sci. Total Environ.* 621, 1074–1083, <https://doi.org/10.1016/j.scitotenv.2017.10.119>.
- Tegelberg, R., 2018. Dry - air drying at room temperature – a practical pre - treatment method of tree leaves for quantitative analyses of phenolics? *January. Phytochem. Anal.* 29, 493–499. <http://dx.doi.org/10.1002/pca.2755>.
- Tovar, G.I., Briceño, S., Suarez, J., Flores, S., González, G., 2020. Biogenic synthesis of iron oxide nanoparticles using *Moringa oleifera* and chitosan and its evaluation on corn germination. *Environ. Nanotechnol. Monit. Manage.* 14, 100350, <https://doi.org/10.1016/j.enmm.2020.100350>.
- United States Environmental Protection Agency (USEPA), 1996. Method 3050B: Acid Digestion of Sediments, Sludges, and Soils, Revision 2. Washington, DC.
- United States Environmental Protection Agency (USEPA), 2003. Method 8015D (SW-846): Nonhalogenated Organics Using GC/FID, Revision 4. Washington DC.
- Usman, M., Faure, P., Hanna, K., Abdelmoula, M., Ruby, C., 2012. Application of magnetite catalyzed chemical oxidation (fenton-like and persulfate) for the remediation of oil hydrocarbon contamination. *Fuel* 96, 270–276, <https://doi.org/10.1016/j.fuel.2012.01.017>.
- Usman, M., Hanna, K., Faure, P., Lorraine, U. De, Nancy, F., 2018. Remediation of oil-contaminated harbor sediments by chemical oxidation. *Sci. Total Environ.* 634, 1100–1107, <https://doi.org/10.1016/j.scitotenv.2018.04.092>.
- Vasantharaj, S., Sathiyavimal, S., Senthilkumar, P., Lewisoscar, F., 2019. Biology biosynthesis of iron oxide nanoparticles using leaf extract of *Ruellia tuberosa*: Antimicrobial properties and their applications in photocatalytic degradation. *J. Photochem. Photobiol. B: Biology* 192, 74–82, <https://doi.org/10.1016/j.jphotobiol.2018.12.025>.
- Wei, X., Gao, N., Li, C., Deng, Y., Zhou, S., Li, L., 2016. Zero-valent iron (ZVI) activation of persulfate (PS) for oxidation of bentazon in water. *Chem. Eng. J.* 285, 660–670, <https://doi.org/10.1016/j.cej.2015.08.120>.
- Xiao, Z., Yuan, M., Yang, B., Liu, Z., Huang, J., Sun, D., 2016. Plant-mediated synthesis of highly active iron nanoparticles for Cr (VI) removal: Investigation of the leading biomolecules. *Chemos* 150, 357–364, <https://doi.org/10.1016/j.chemosphere.2016.02.056>.
- Zabbey, N., Sam, K., Trinitas, A., 2017. Environment remediation of contaminated lands in the niger delta, nigeria: prospects and challenges. *Sci. Total Environ.* 586, 952–965, <https://doi.org/10.1016/j.scitotenv.2017.02.075>.
- Zheng, L., Zhao, Y., Lin, Y., Li, C., 2016. Heat-activated persulfate oxidation of dinotefuran in water. *Chin. J. Environ. Eng.* 10 (6), 2992–2996, <https://doi.org/10.12030/j.cjee.201501113>.